NUCLEAR STRUCTURE -- EXPERIMENTAL

NEUTRON UNSTABLE ^{10}Li PRODUCED BY FRAGMENTATION

R. A. Kryger, A. Azhari, A. Galonsky, J. H. Kelley, R. Pfaff, E. Ramakrishnan, D. Sackett[a], B. M. Sherrill, M. Thoennessen, J. A. Winger, and S. Yokoyama.

The experimental study of the structure of very neutron- and proton-rich nuclei provides new insight into the properties of nuclear matter and unique tests for nuclear models. This is true not only for the long-lived radioactive nuclei that undergo β-decay, but also for the particle-unstable nuclei just beyond the driplines. We have applied the technique of Sequential Neutron Decay Spectroscopy[1] (SNDS) to fragmentation reaction products produced near 0° in order to investigate the structure of light nuclei beyond the neutron dripline. The SNDS method detects colinear neutron-fragment coincidences from the decay of neutron unbound states. The decay energy E of the parent state is related to the relative velocity v_{rel} of the neutron and fragment by means of the (non-relativistic) relationship $E = \frac{1}{2}\mu v_{rel}^2$ where μ is the reduced mass of the neutron and fragment system. By extending this method to fragments produced near 0° we take advantage of kinematic focussing in the intermediate energy fragmentation reaction. As a first case, we have focussed on the neutron-unbound nucleus ^{10}Li because of the uncertainty concerning the ground state mass and its importance to the understanding of the halo nucleus ^{11}Li.

The experiment was performed using an 80 MeV/nucleon ^{18}O beam from the K1200 Cyclotron incident upon a 9 mg/cm^2 ^{nat}C target. Reaction products were momentum analyzed by a section of the beamline consisting of two quadrupole magnets followed by a dipole magnet, used as a magnetic spectrometer. Fragments with a mass-to-charge ratio equal to 3 were bent to 11° and focussed onto a phoswich fragment detector. The primary beam was bent to 14° by the dipole magnet and dumped approximately 10 m downstream behind more than 1 m of concrete shielding. The phoswich fragment detector was a 10.2 cm diam cylinder consisting of a 3 mm thick NE102A fast plastic layer and a 9.5 cm thick NE115 slow plastic layer. Light output was detected via two phototubes coupled to the back of the detector. Energy-loss (ΔE) in the fast plastic and total energy (E) were determined by integrating the charge in the phototube output pulses over narrow and wide time gates. Fragment time-of-flight (TOF) was determined relative to the accelerator RF, and particle identification (both A and Z) was accomplished by means of the ΔE, E, and TOF signals. Fragment velocity was determined from the TOF and the target-to-detector flight path of 6.0 m. Neutrons were detected directly at 0° in three 6.3 cm diam by 7.6 cm cylindrical NE-213 or BC501 liquid scintillator detectors placed 5.0 m from the target. Neutron velocity was determined from the neutron TOF, and the timing resolution for both neutron and fragment TOF was 2.1 ns (FWHM). Pulse shape discrimination and TOF cuts were used offline to remove the γ-ray background events. Relative velocity spectra were formed from the coincident neutron-fragment events separately for each fragment isotope, and the spectra were corrected for the random coincidence background. Shadowbar measurements were also made and the scattered neutron background, found to account for less than 5% of the random-corrected coincidence data, was subtracted.

Figure 1 shows the relative velocity spectrum for coincident neutron + ^{6}He events which were obtained simultaneously with the n + ^{9}Li data. The data show two peaks at $v_{rel} \approx \pm 0.8$ cm/ns superimposed upon a broad background. The peaks correspond to the decay of the known particle-unstable ^{7}He ground state ($E_r = 0.45 \pm 0.03$ MeV, $\Gamma = 0.16 \pm 0.03$ MeV), where the neutron is emitted near either 0° or 180° with respect to the incident beam. We have modeled the background under the peaks using a gaussian lineshape and the result is shown by the dashed line in the Figure. The solid line shows the calculated spectrum for the ^{7}He decay using a Breit-Wigner decay lineshape and a Monte Carlo simulation to account for detector acceptances

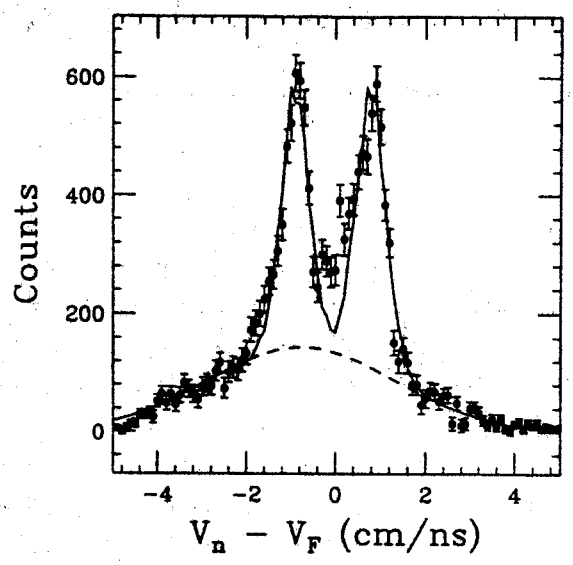

Figure 1: The relative velocity spectrum for n + ^{6}He coincidence events. The dashed line shows the estimated background and the solid line is the result of the simulated decay of ground state ^{7}He.

and efficiencies as well as the experimental time resolution. The colinear detection geometry is found to be particularly sensitive to the low energy part of the decay lineshape because of the high coincidence detection efficiency for low relative-energy events.

Figure 2 shows the relative velocity data for the n + ^{9}Li coincidence events. These data are dominated

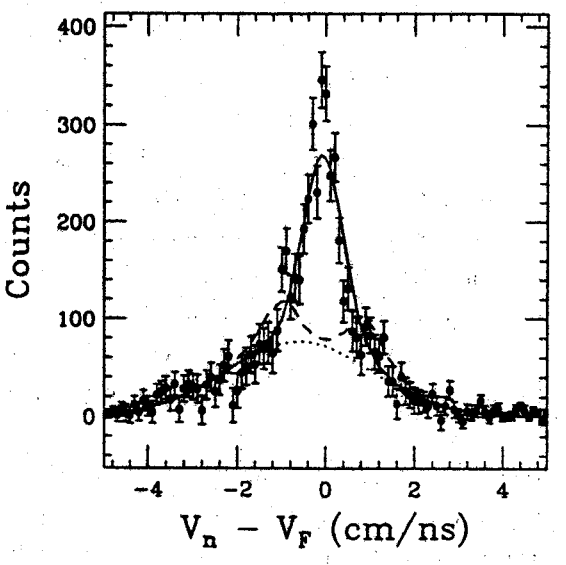

Figure 2: The relative velocity spectrum for n + ^{9}Li coincidence events. The dotted line shows the estimated background and the solid line is the result of the simulated decay of the ^{10}Li ground state reported by Amelin, *et al.*[3]. The dashed line is the result of a calculation for the ^{10}Li state reported by Wilcox, *et al.*[4].

by a single peak near 0 cm/ns arising from the emission of a low-energy neutron from the ^{10}Li system. The estimated background in this data is shown by the dotted line. The solid and dashed lines show the result of calculations for the two previously published ^{10}Li ground state decay parameters. The dashed line corresponds to the spectrum for the E_r = 800 keV (Γ = 1.2 MeV) state reported by Wilcox *et al.* [2] and the solid line corresponds to a decay with E_r = 150 keV (Γ = 400 keV) consistent with the limits established by the more recent results of Amelin, *et al.* [3]. There is some evidence for the Wilcox state in the data near ±1 cm/ns, but the central peak is more consistent with the Amelin results. However, it is not possible to conclude from the present data that we are observing the decay of the ^{10}Li ground state since the SNDS method only determines the relative energy between decay products. It is possible that the observed peak corresponds to an excited ^{10}Li state decaying to the first-excited ^{9}Li state at E_x = 2.69 MeV (the only particle-bound excited state in ^{9}Li). In this case, the excitation energy of the ^{10}Li state would be approximately $E_x \approx 2.5$ MeV. A more detailed discussion of this analysis has been submitted for publication[4].

a. Present Address: Niton Corporation, 74 Loomis St., Bedford, MA 01730.

References

1 F. Deak, A. Kiss, Z. Seres, G. Caskey, A. Galonsky, and B. Remington, Nucl. Instrum. Methods **A258**, 67 (1987).
2 K. H. Wilcox, R. B. Weisenmiller, G. J. Wozniak, N. A. Jelley, D. Ashery, and J. Cerny, Phys. Lett. **B59**, 142 (1975).
3 A. I. Amelin, M. G. Gornov, Yu. B. Gurov, A. L. Ilín, P. V. Morokhov, V. A. Pechkurov, V. I. Savelév, F. M. Sergeev, S. A. Smirnov, B. A. Chernyshev, R. R. Shafigullin, and A. V. Shishkov, Sov. J. Nucl. Phys. **52**, 782 (1990).
4 R. A. Kryger *et al.*, submitted to Phys. Rev. C.

ELECTROMAGNETIC EXCITATION OF ^{11}Li

A. Galonsky, D. Sackett, K. Ieki, C.A. Bertulani, H. Esbensen, J.J. Kruse, W.G. Lynch, D.J. Morrissey, N.A. Orr, B.M. Sherrill, H. Schulz, A. Sustich, J.A. Winger, F. Deák[a], Á. Horváth[a], Á. Kiss[a], Z. Seres[b], J.J. Kolata[c], R.E. Warner[d], and D.L. Humphrey[e]

We have performed a kinematically complete measurement of the Coulomb dissociation of 28 MeV/nucleon ^{11}Li into ^{9}Li and two neutrons by a Pb target [1]. From the energies and angles of the emitted neutrons and of ^{9}Li, the excitation energy E of ^{11}Li was determined on an event-by-event basis, and the Coulomb dissociation cross section was constructed. In Fig. 1(a), the experimentally obtained Coulomb dissociation cross section is displayed as a function of decay energy E_d. The excitation energy is related to E_d by $E = E_d + S_{2n}$, where S_{2n} is the 2-neutron separation energy of ^{11}Li. The data in this figure have not been corrected for the dependence of the detector's solid-angle acceptance on E_d. The solid line in Fig. 1(a) results from a Monte Carlo simulation which fully takes into account the finite geometry and finite resolution of the detector and which assumes a Lorentz-type photonuclear cross section $\sigma_{E1}(E_d)$, as shown in Fig 1(b). $\sigma_{E1}(E_d)$ has a peak at E_d=0.7 MeV and a width $\Gamma = 0.8$ MeV. These parameters are consistent with the picture of a soft dipole mode [2].

However, a significant difference was observed between the velocity distributions of neutrons and ^{9}Li, i.e., in general, ^{9}Li has a larger velocity than the neutrons (Fig. 2). This fact is understood if the breakup occurs within the strong Coulomb field of the Pb target. The observed velocity difference limits the lifetime of the excited ^{11}Li nucleus to be about 50 fm/c. Such a short lifetime is in contradiction with the small width of the $\sigma_{E1}(E_d)$ peak if we interpret that peak as a soft dipole resonance. The short lifetime, instead, favors a direct breakup picture.

The complete kinematical measurement also allowed neutron and ^{9}Li momentum distributions to be constructed in the rest frame of the ^{11}Li (Fig. 3). The momentum distributions can be fitted with Gaussian functions, yielding width parameters $\sigma_9 = 18 \pm 4$ MeV/c and $\sigma_n = 13 \pm 3$ MeV/c. These distributions are both in good agreement with previous measurements of the neutron angular distribution [3] and the ^{9}Li longitudinal momentum distribution [4]. A more general feature of the breakup mechanism of ^{11}Li could be deduced from these measurements. It was found that the ^{9}Li and neutron momentum distributions and the neutron-neutron relative momentum distribution could be reproduced if the ^{11}Li decay energy was partitioned between the ^{9}Li and the neutrons by a 3-body phase space distribution at the breakup as shown by the histograms in Fig. 3. This agreement also indicates that there is *no* directional correlation, such as that suggested by Tanihata *et al.* [5], between the emitted neutrons.

a. Department of Atomic Physics, Eötvös Loránd University, Puskin utca 5-7, H-1088 Budapest 8, Hungary.
b. KFKI Research Institute for Particle and Nuclear Physics of the Hungarian Academy of Sciences, H-1525 Budapest 114, Hungary.
c. Department of Physics, University of Notre Dame, Notre Dame, Indiana 46556.
d. Department of Physics, Oberlin College, Oberlin, Ohio 44074.
e. Department of Physics, Western Kentucky University, Bowling Green, Kentucky 42101.

References

1. K. Ieki *et al.*, Phys. Rev. Lett. **70**, 730 (1993);
D. Sackett *et al.*, Phys. Rev. **C**, submitted.
2. T. Kobayashi *et al.*, Phys. Lett. **B232**, 51 (1989);
K. Ikeda, Nucl. Phys. **A538**, 355c (1992).

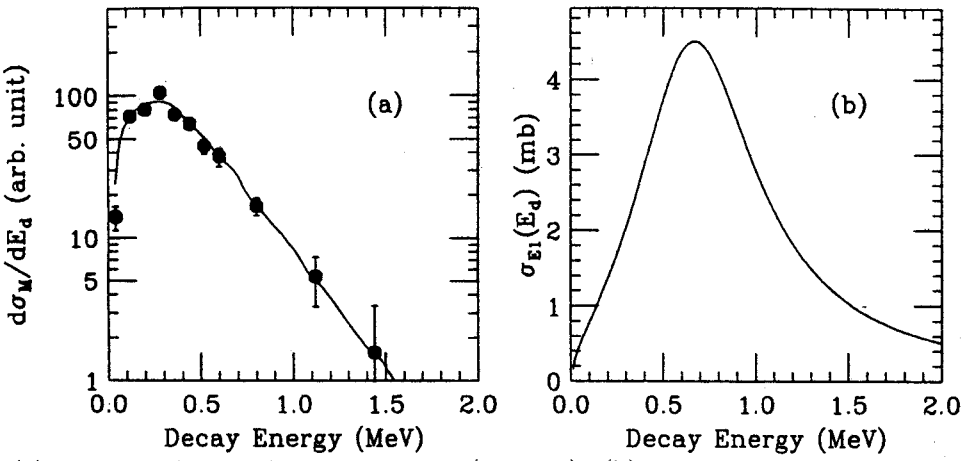

Figure 1: (a) Coulomb dissociation cross section (see text). (b) Lorentz-type distribution for $\sigma_{E1}(E_d)$ used in the Monte Carlo simulation which fits the data (solid line in (a)).

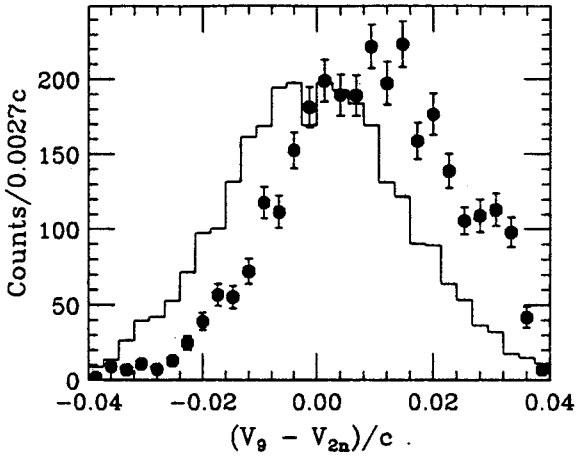

Figure 2: Velocity difference between ^{9}Li and neutrons. Histogram results from a Monte Carlo simulation without the Coulomb acceleration effect.

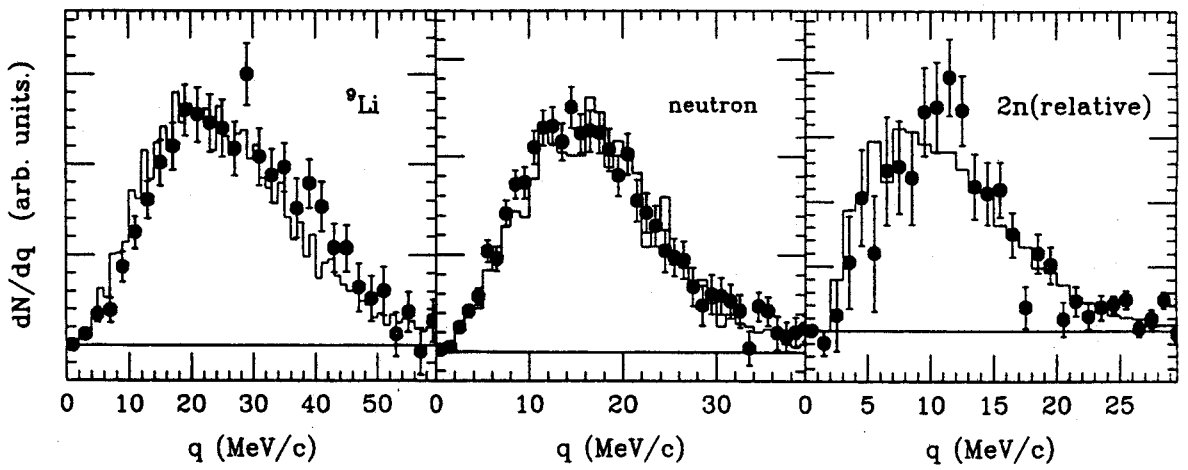

Figure 3: Momentum distributions for ^{9}Li(left) and neutron(center) in the c/m frame of ^{11}Li, and neutron-neutron relative momentum(right). Histograms result from the Monte Carlo simulation which assumes a 3-body phase space distribution.

THE MOMENTUM DISTRIBUTION OF ^{10}Be FRAGMENTS FROM THE BREAKUP OF ^{11}Be

J.H. Kelley, Sam M. Austin, R.A. Kryger, D.J. Morrissey, N.A. Orr, B.M. Sherrill, M. Thoennessen, J. S. Winfield and J.A. Winger.

We have measured the parallel momentum distribution of ^{10}Be fragments from the breakup of ^{11}Be nuclei on a range of targets (Z = 4 - 92). A ^{11}Be beam produced by the fragmentation of an ^{18}O beam in a thick Be target bombarded a breakup target located at the secondary image of the A1200, producing ^{10}Be fragments. The Momentum distributions exhibit narrow structures (FWHM $\approx$ 43 MeV/c), showing little target dependence.

The momentum distribution of fragments following a direct breakup is expected to reflect the momentum distribution of those fragments in the nucleus prior to the breakup. Thus a measurement of the momentum distribution of ^{10}Be fragments from the 2-body breakup of ^{11}Be should yield the momentum distribution of the valence neutron in ^{11}Be before the breakup. From the uncertainty principle, a narrow momentum distribution width indicates an extended spacial distribution. For a typical stable nucleus like ^{12}C [1], fragments have momentum distributions with Gaussian widths of 100-150 MeV/c, while widths as narrow as 19 MeV/c [2] are observed for fragments from weakly bound nuclei, indicating a very different structure for the outer neutrons - a neutron halo.

In principle both the parallel and transverse momentum distributions are useful for determining the spacial distribution of outer neutrons. However the transverse momentum distribution is perturbed by the effects of multiple scattering. Coulomb deflection and diffractive broadening. Parallel momentum distributions are not influenced by these effects [3]. although for a thick breakup target, energy straggling in the target acts to broaden the momentum distribution. In our case, the size of the broadening can be measured and is subtracted from the fragment momentum distribution width in quadrature resulting in only a 5 % correction (reduction) in width.

^{11}Li has been the subject of detailed investigation following measurements of very large total reaction and Coulomb breakup cross sections. Other experiments, including those of Ieki et al. [4] and Orr et al. [2], have shown that ^{9}Li fragments from ^{11}Li have narrow structures in their momentum distributions (Gaussian $\sigma \approx$ 19 MeV/c). Orr et al. observed a slight target dependence for the width of the ^{9}Li fragment momentum distribution possibly indicating dependence on the breakup mechanism (nuclear breakup - Be, Coulomb breakup - Ta). Interpretation of the 3-body breakup of ^{11}Li to ^{9}Li and two neutrons is complicated by the possibility of both simultaneous breakup and of sequential decay through the unbound ^{10}Li nucleus. Desire to study a simpler two-body system has led to the ^{11}Be nucleus ($S_n = 504 \pm 6$ keV), an expected 1-neutron halo nucleus. Reaction cross section measurements [5] indicate that ^{11}Be has an extended neutron distribution, and a measurement of the momentum distribution of ^{10}Be fragments from the breakup of ^{11}Be could provide more direct evidence on the nature of the neutron halo.

As a zero degree energy loss spectrometer the A1200 provided a resolution of 0.15 % for measuring the momentum distribution of ^{10}Be fragments, in spite of a 1.0 % spread in ^{11}Be momentum. For the measurement, a beam of 80 MeV/u ^{18}O from the K1200 cyclotron bombarded a thick 790 mg/cm^2 Be production target, located at the A1200 target pot (medium acceptance mode), producing a beam of ^{11}Be fragments. The first set of dipoles in the A1200 selected fragments with a rigidity of 3.109 T-m (^{11}Be with 62.8 MeV/A) optimizing the transmission rate of ^{11}Be ions with a rate of 331 sec^{-1} (pnA of ^{18}O)$^{-1}$ of primary beam. An aperture located at

the first dispersive image limited the momentum spread of the secondary beam to ± 0.5 %. A target located at the second dispersive image induced a breakup of the ^{11}Be ions leading to ^{10}Be fragments having a momentum distribution peaked around 3400 MeV/c. The rigidity of the second half of the A1200 was 2.900 T-m, permitting the ^{10}Be breakup fragments to reach the final focal plane.

In the final focal plane particles are detected by a standard A1200 detector setup consisting of two 2-dimensional position sensitive Parallel Plate Avalanche Counters (PPAC's), a gas ionization drift chamber for ΔE and a thick plastic stopping detector for timing against the cyclotron rf-signal. The ^{10}Be breakup fragments are identified by their time of flight through the A1200 and ΔE, while their momentum is determined by position in the focal plane.

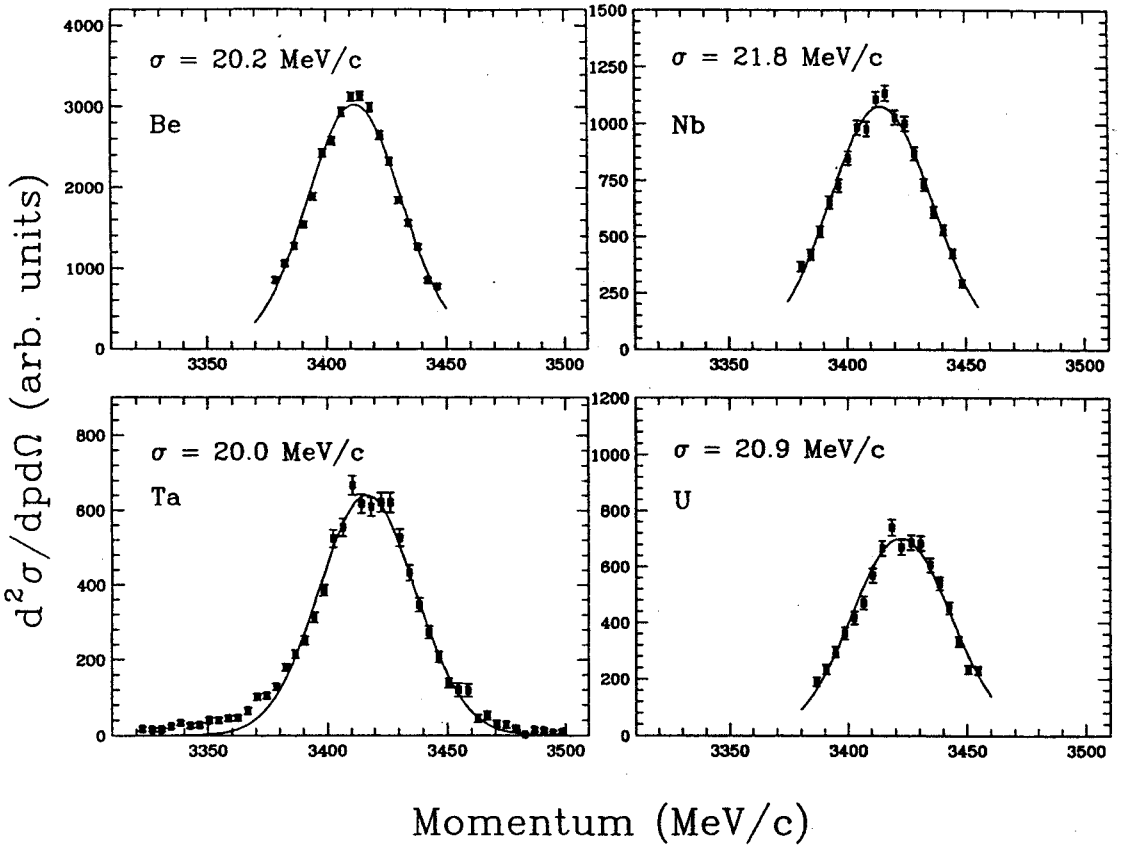

Figure 1: The central 2% of the momentum distribution of ^{10}Be fragments following the breakup of ^{11}Be on Be, Nb and U targets. The central 5% of the momentum distribution is shown for the Ta target with a Gaussian fitted to the central 2% (σ = 20.0 MeV/c preliminary).

The data (figure 1), corrected for efficiency of transmission through the A1200, show momentum distributions with Gaussian widths $\sigma \approx 21$ MeV/c. Additional corrections for target effects and a transformation to the center of mass frame are necessary to obtain a momentum distribution representative of the valence neutron's momentum distribution in ^{11}Be. The efficiency for transmission as a function of momentum is determined by stepping a beam of known rigidity across the focal plane and normalizing to the beam current.The momentum calibration for the focal plane is obtained simultaneously. A beam of 62.3 MeV/u ^{10}Be ions was used to measure the target thickness by the energy loss in the target. By passing a beam of ^{10}Be through the Image 2 breakup targets and measuring the resulting spread in momentum at the focal plane the resolution is obtained. The resolution, which is subtracted in quadrature from the width of momentum distribution of ^{10}Be fragments from

^{11}Be, includes the spectrometer resolution, detector resolution, and target effects that act to broaden the distribution (ie. energy straggling in the thick breakup targets). The transformation to the center of mass frame reduces the width by a factor of γ, the relativistic correction factor. In the ^{11}Be rest frame Gaussian fits to the data have momentum distribution widths of $\sigma \approx 19.5$ MeV/c.

The data presented represents the central 2% of the ^{10}Be fragment momentum distribution for Be, Nb and U targets. Sampling over the central 5% of the momentum distribution for the Ta target permits a better evaluation of the wings of the distribution. A Gaussian distribution, fit to the central 2% of the distribution is plotted for the Ta target. The low momentum side is not well fit, though it is not surprising to see a low momentum tail in the momentum distribution for fragments from light nuclei. Contaminants in the secondary beam, like ^{13}B, ^{14}B, ^{16}C and ^{17}C, could produce ^{10}Be fragments that would be indistinguishable from fragments from ^{11}Be. However, these contaminants would give the momentum distribution a nearly flat background. The centroid for ^{10}Be fragments from ^{14}B should be at 3333 MeV/c, so ^{14}B could contribute to the low momentum enhancement of the distribution. Contributions from other contaminants do not appear to be large, and should be small since centroids for their ^{10}Be fragments are further from the peak for fragments from ^{11}Be.

Studies of the limited acceptance for ^{10}Be breakup fragments from the secondary target at image 2 have shown that an acceptance limit may influence the width of the momentum distribution. Private communications with K. Riisager [6] show that the affect on the distribution is related to the line of the distribution. For example, the parallel component of a Gaussian distribution will not change in shape or width when subjected to a limited acceptance at these energies, however a Lorentzian distribution will show a dependance on the acceptance. In a simplified picture, a limited acceptance represents an integration over a limited range of the transverse components. Since the form of the momentum distribution remains unclear, we present our results as a measure of the Full Width at Half Maximum height (FWHM = 2.355 σ).

Target	Uncorrected FWHM (MeV/c)	Efficiency Correction (MeV/c)	Resolution Correction (MeV/c)	Corrected FWHM (MeV/c)	^{11}Be Rest Frame (MeV/c)
Be	43	+1.3	-1.0	43	40
Nb	48	+1.8	-1.4	48	45
Ta	48	+1.0	-2.3	47	44
U	46	+1.5	-1.9	46	43

Table 1: Summary of the preliminary results.

In summary, we have measured the parallel momentum distribution for ^{10}Be fragments following the breakup of ^{11}Be. Be, Nb, Ta and U targets were used to sample both the nuclear and Coulomb breakup mechanisms. The momentum distribution exhibits a narrow component with a FWHM of $\approx$ 43 MeV/c, showing little target dependence. The small sensitivity on target supports the view that the momentum distribution reflects information about the halo structure of ^{11}Be, rather than information about the breakup mechanism.

References

1. D.E. Greiner *et al.*, Phys. Rev. Lett. **35**, 152 (1975).
2. N.A.Orr *et al.*, Phys. Rev. Lett. **69**, 2050 (1992).
3. C.A. Bertulani and K.W. McVoy, Phys. Rev. C **46**, 2638 (1992).
4. K.Ieki *et al.*, Phys. Rev. Lett. **70**, 730 (1993).
5. I. Tanihata, Nucl. Phys. A **488**, 113 (1988).
6. K. Riisager, Private communication, November 1992.

MASS MEASUREMENTS OF ^{10}Li AND ^{11}Li

B. M. Young, W. Benenson, G. F. Bertsch [a], B. A. Brown, M. Hellstrom, J. H. Kelley, T. Kubo, N. A. Orr [b], R. Pfaff, B. M. Sherrill, M. Steiner, M. Thoennessen, J. S. Winfield, J. A. Winger [c], S. J. Yennello [c], and A. Zeller.

With the recent advent of intense radioactive nuclear beam production, the region of experimentally obtainable nuclei has greatly expanded to include both drip-lines. This has made possible the study of nuclei far from stability, and has revealed structures and dynamic systems quite unlike those previously studied. Among the more interesting such nuclei is ^{11}Li. A large body of experimental evidence [1–6] has indicated that ^{11}Li consists of a ^{9}Li core and a "halo" of two loosely bound neutrons, the matter radius of which extends well beyond that expected from traditional nuclear models. The fact that ^{11}Li is loosely bound while ^{10}, with one less neutron, is unbound implies that the interaction between the valence neutrons of ^{11}Li plays a vital role in its stability and structure. With these ideas as a starting point, several calculations have been made by treating ^{11}Li as a three-body system comprising a ^{9}Li core and 2 neutrons [7–10]. Central to these models is the interaction of a single neutron and the ^{9}Li core. For this reason, there is also considerable interest in the unbound nucleus ^{10}Li.

It is expected that the lowest states of ^{10}Li should consist of the valence proton in the $1p\frac{3}{2}$ orbit combined with the seventh neutron in the $1p\frac{1}{2}$ or the $2s\frac{1}{2}$ orbits. Such a configuration would lead to four states of ^{10}Li having J^{π} values of 1^+, 1^-, 2^+, and 2^-. In the first measurement of the ^{10}Li mass, Wilcox *et al.* [11] determined the coincident energies of ^{8}B and ^{9}Li (from the breakup of ^{10}Li) produced in the reaction ^{9}Be(^{9}Be,^{8}B)^{10}Li at 121 MeV. They observed a state with $S_n = -0.80 \pm 0.25$ MeV and $\Gamma_{c.m.} = 1.2 \pm 0.3$ MeV. It was assumed that this was the ground state of ^{10}Li. Soon thereafter, Barker and Hickey [12] argued that the ^{10}Li ground state should be narrrow and much less unbound to neutron decay and should be one of the $\nu 2s\frac{1}{2}$ states. They further suggested that the state observed by Wilcox *et al.* was one of the broader $\nu 1p\frac{1}{2}$ states. In 1990, Amelin *et al.* [13] measured the inclusive spectrum of protons produced in absorption of π^- by ^{11}B nuclei and reported the observation of a state in ^{10}Li unbound to neutron decay by approximately 150 keV. The existence of a weakly unbound $\nu 2s\frac{1}{2}$ ground state would be in agreement with the suggestions of Barker and Hickey, as well as the theoretical predictions of Warburton and Brown [14]. Also supporting the existence of this state is the observation by Abramovich *et al.* of a $T = 2$ state in ^{10}Be [15]. However, this state has yet to be clearly observed [16] since the original report by Amelin *et al.*. Very recently, Bohlen *et al.* [17] have reported their observation of a 1^+ ground state with mass excess 33.445 ± 0.050 MeV and an excited state with excitation energy 0.38 ± 0.08 MeV. This corresponds to two $\nu 1p\frac{1}{2}$ resonances with separation energies of -0.420 ± 0.050 and -0.800 ± 0.094 respectively. Clearly there is a discrepancy regarding the nature of the ground and first two excited states of ^{10}Li.

In May of 1992, momentum spectra were obtained from the reaction ^{11}B(^{7}Li,^{8}B)^{10}Li. The experiment was performed with an $E/A = 18.6$ MeV, ^{7}Li^{1+} beam from the K1200 cyclotron at the National Superconducting Cyclotron Laboratory. The target was a self-supporting ^{11}B foil 0.125 mg/cm^2 thick. A ^{12}C (natural) target, 0.56 mg/cm^2 thick, was used for the calibration runs. The reaction products were analyzed with the S320 magnetic spectrograph with a resolution of 0.23 MeV. The focal plane detector consisted of two resistive wire position counters separated by two ionization chambers. The ions were stopped in a thick plastic scintillator. The energy loss signal from the ionization chambers and the time-of-flight, taken from the scintillator signal relative to the cyclotron rf, provided unambiguous particle identification. The position counters at the spectrometer focal plane were calibrated by setting the magnetic elements to step elastically scattered beam particles across

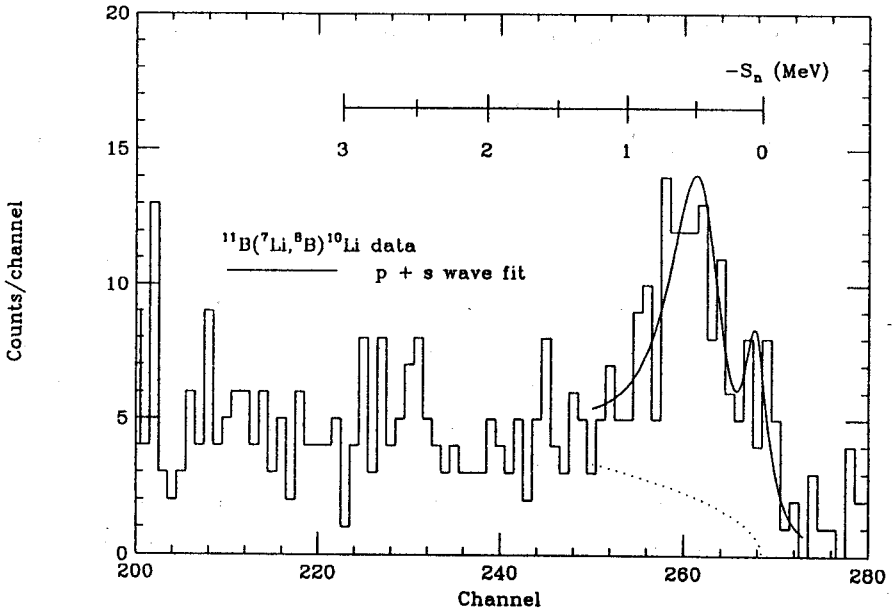

Figure 1: The momentum spectrum collected from the reaction $^{11}B(^7Li,^8B)^{10}Li$. There is a slight knee in the broad peak at $S_n \geq -100$ keV which may correspond to a $2s\frac{1}{2}$ ground state of ^{10}Li. The broader peak centered at $S_n \simeq -500$ keV contains at least one $1p\frac{1}{2}$ state of ^{10}Li. The best fit to the data, shown with the solid line, was obtained with one p–wave resonance, one s–wave resonance, and a 3–body background. The line shape for the p–wave is obtained from neutron resonance calculations described in Ref. 18. The narrow state is taken to be an s–wave neutron state, the line shape of which is assumed to be a Lorentzian with width 230 keV. The 3–body background is shown in dots. The fitting procedure was a maximum likelihood technique also described in Ref. 18.

the active area of the detector array. These points were fit with a second–order polynomial. Also, spectra were collected for $^{12}C(^7Li,^8B)^{11}Be$ at the same angles and field settings as the reaction measurements. The resolved low–lying states in ^{11}Be were used to fix the calibration for the ^{10}Li spectrum.

Figure 1 shows the momentum spectrum collected from the reaction $^{11}B(^7Li,^8B)^{10}Li$ at a laboratory angle of 5°. The most striking feature of this data is the broad peak corresponding to a neutron separation energy of approximately −500 keV. There is also a slight narrow enhancement in the broad peak at $S_n \geq -100$ keV. The lowest neutron states of ^{10}Li are expected to be either s–wave or p–wave resonances. More specifically, calculations performed by Warburton and Brown indicate that the ^{10}Li ground state should have the valence neutron in the $2s\frac{1}{2}$ orbit and the first and second excited states should both have $1p\frac{1}{2}$ valence neutron orbits. Since low energy s–wave neutron resonances are expected to be narrow, the observed broad peak is believed to correspond to one or more p–wave resonances, while the narrower, less unbound peak could be an s–wave resonance belonging to the ^{10}Li ground state. Resonance scattering calculations have been performed to estimate the widths and line shapes of s– and p–wave resonances. These calculations are described in detail in Ref. 18. It was found that resonances for low lying ($S_n \geq -200$ keV) $2s\frac{1}{2}$ neutrons in a ^9Li well are narrower than 0.23 MeV, so the device resolution shape was used in the fits. The line shape, in particular the width and assymetry of the peak, was parametrized as a function of resonance energy for $1p\frac{1}{2}$ neutrons. This parametrization, in addition to a 3–body phase space distribution from the reaction $^{11}B(^7Li,^8B)^9Li+n$, was also used in the fits. Since the statistics in the collected spectrum are so low, the standard least–squares fitting technique is inapplicable. Instead, an analogous method [18] was used which assumed that the data had a Poisson distribution about the theoretical model.

The best agreement with the data was obtained with a single $1p\frac{1}{2}$ neutron resonance at a Q–value of -32856 ± 55 keV ($S_n(^{10}\mathrm{Li}) = -486 \pm 55$ keV) with a width $\Gamma_{\mathrm{lab}} = 377 \pm 17$ keV, and a narrow $2s\frac{1}{2}$ neutron resonance at a Q–value greater than -32471 keV ($S_n(^{10}\mathrm{Li}) \geq -100$ keV) with width $\Gamma_{\mathrm{lab}} \leq 230$ keV. This fit is shown with the solid line in Figure 1. An attempt was also made to fit the data with two p–wave resonances. Reasonable fits were obtained only by placing the resonances less than 160 keV apart and centered near -485 keV separation energy. It is important to note that under no circumstances could a reasonable fit be made with a resonance unbound by more than 600 keV. Both of these results, the possibile existence of a low–lying $2s\frac{1}{2}$ neutron state, and the fact that the broad peak in the data can only be fit by a single $1p\frac{1}{2}$ neutron resonance or by two such resonances separated by less than 160 keV, are in contradiction with the results of Bohlen *et al.*. A possible explanation for the discrepancy in the number and location of the p–wave neutron resonances is that Bohlen *et al.* assumed Gaussian line shapes, the widths of which were obtained from R–matrix calculations. The line shapes obtained in the calculations described above were broader than those used by Bohlen *et al.* and were highly asymmetric. It is possible that the narrowness and unrealistic lack of asymmetry of the line shapes used by Bohlen *et al.* artificially necessitated the presence of the state at $S_n \simeq -800$ keV. Another explanation could be that the more highly unbound $1p\frac{1}{2}$ neutron state does exist, but was not populated by the reaction studied in the present work. It must also be stated that the evidence for the $2s\frac{1}{2}$ state is less than conclusive. It is possible that, if this state exists, the reactions studied by Bohlen *et al.* did not populate it strongly enough to be observed. It is clear that further experimental effort is greatly needed to solve this puzzle.

It is essential, in order to gauge the validity of calculations of the type described in Refs. 7–10, to have accurate measurements of the observables predicted by these models. One of the most basic observables is the mass or, equivalently, the two–neutron separation energy of ^{11}Li. The most recent measurement, by Kobayashi *et al.* [19], is $S_{2n}(^{11}\mathrm{Li}) = 340 \pm 50$ keV. In late September of 1992, momentum spectra were collected from the reaction $^{14}\mathrm{C}(^{11}\mathrm{B},^{11}\mathrm{Li})^{14}\mathrm{O}$. An $E/A = 32.05$ MeV, $^{11}\mathrm{B}^{2+}$ beam from the K1200 cyclotron was collided with a self–supporting ^{14}C foil 0.45 mg/cm^2 thick, located in the high–acceptance target pot of the A1200 fragment separator. The reaction products were analyzed with the A1200 operating in high–acceptance chromatic mode. The A1200 focal plane detectors consisted of one PPAC, a 0.5mm thick Si position–sensitive detector, and a scintillating plastic stopping detector. Redundant and unambiguous particle identification was obtained by combining the energy loss signal from the silicon detector with the total energy signal from the plastic and with the time–of–flight information obtained from the scintillator signal relative to the cyclotron rf. The position–sensitive detector was calibrated at several spectrometer field settings with the reaction $^{14}\mathrm{C}(^{11}\mathrm{B},^{9}\mathrm{Li})^{16}\mathrm{O}$. Also, the reaction $^{14}\mathrm{C}(^{11}\mathrm{B},^{10}\mathrm{Be}^{3+})^{15}\mathrm{N}^*$, where the ground and 5.3 MeV excited states of ^{15}N were observed, provided a calibration at the same spectrometer field settings as those used for the production reaction. The spectrum from this reaction is shown in the top part of Figure 2. The collected spectrum from the reaction $^{14}\mathrm{C}(^{11}\mathrm{B},^{11}\mathrm{Li})^{14}\mathrm{O}$ is shown in the bottom part of Figure 2. Preliminary analysis indicates a value of $S_{2n}(^{11}\mathrm{Li}) = 320$ keV, in agreement with the value reported by Kobayashi *et al.*.

a. Current address: Dept. of Physics, Univ. of Washington, Seattle, Washington.
b. Current address: GANIL, Caen, France.
c. Current address: Cyclotron Institute, College Station, Texas.

References

1. N. A. Orr *et al.*, Phys. Rev. Lett. **69**, 2050 (1992).
2. T. Kobayashi *et al.*, Phys. Rev. Lett. **60**, 2599 (1988).
3. K. Riisager *et al.*, Nucl. Phys. **A540**, 365 (1992).

4. R. Anne *et al.*, Phys. Lett. B **250**, 19 (1990).
5. T. Kobayashi *et al.*, Phys. Lett. B **232**, 51 (1989).
6. B. Blank *et al.*, Z. Phys. A **340**, 41 (1991).
7. H. Esbensen and G. F. Bertsch, Nucl. Phys. A (to be published).
8. G. F. Bertsch and H. Esbensen, Ann. Phys. (N.Y.) **209**, 327 (1991).
9. M. V. Zhukov *et al.*, Phys. Lett. B **265**, 19 (1991).
10. L. Johannsen, A. S. Jensen, and P. G. Hansen, Phys. Lett. B **244**,357 (1990).
11. K. H. Wilcox *et al.*, Phys. Lett. B **59**, 142 (1975).
12. F. C. Barker and G. T. Hickey, J. Phys. G: Nucl. Phys **3**, L23 (1977).
13. A. I. Amelin *et al.*, Sov. J. Nucl. Phys. **52**, 783 (1990).
14. E. K. Warburton and B. A. Brown, Phys. Rev. C **46** 923 (1992).
15. S. N. Abramovich *et al.* Bull. Acad. Sci. USSR, Phys. Ser. **37**, 144 (1973).
16. R. Kryger *et al.*, Phys. Rev. C (in press).
17. H. G. Bohlen *et al.*, Z. Phys. A **344**, 381 (1993).
18. B. M. Young *et al.*, to be published.
19. T. Kobayashi *et al.*, KEK Report No. 91-22, 1991 (to be published).

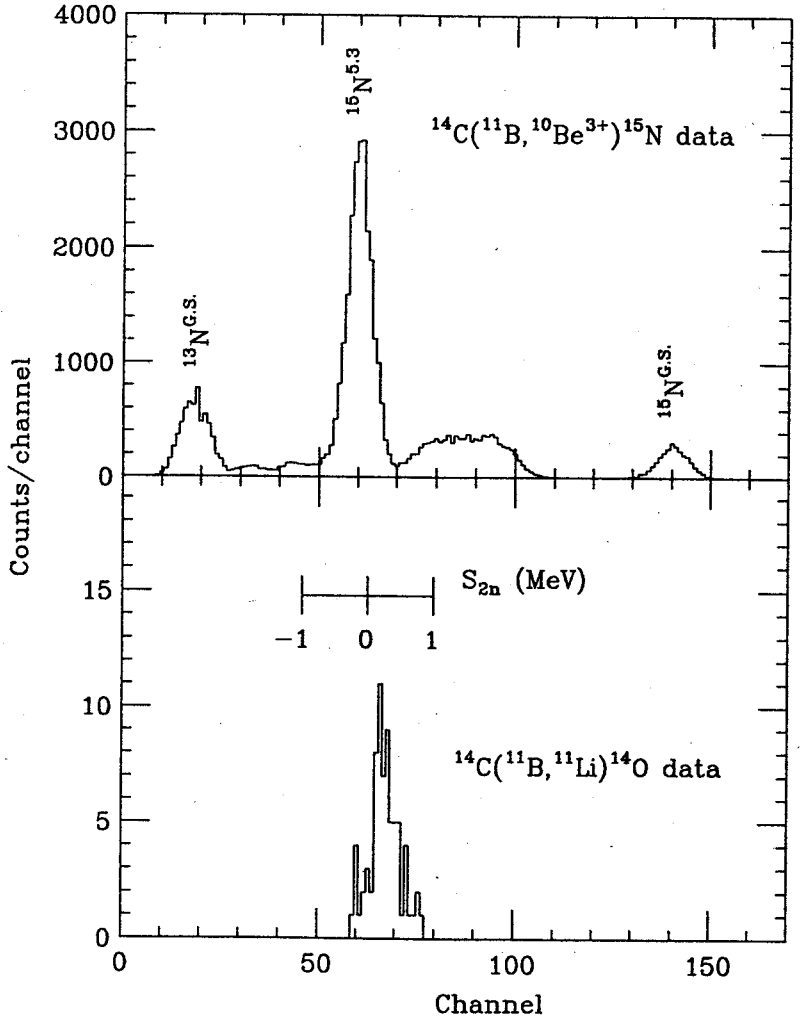

Figure 2: The momentum spectrum from the reaction $^{14}C(^{11}B,^{10}Be^{3+})^{15}N^*$ is shown in the bottom part of the figure. The ground state and 5.3 MeV doublet states of ^{15}N were used as the primary calibration points. The momentum spectrum collected from the reaction $^{14}C(^{11}B,^{11}Li)^{14}O$. It is important to note that both spectra were collected simultaneously. Preliminary analysis indicates a value of $S_{2n}(^{11}Li) = 320$ keV. This is in agreement with the value reported in Ref. 19.

EVIDENCE FOR LONG FORMATION TIMES OF NEAR BARRIER FUSION REACTIONS

M. Thoennessen, J. R. Beene[a], F. E. Bertrand[a], C. Baktash[a], M. L. Halbert[a], D. J. Horen[a], D. G. Sarantites[b], W. Spang[c], and D. W. Stracener[b].

It is well established that dissipative effects influence the reaction dynamics of heavy-ion collisions. Swiatecki [1] developed a dissipative collision model which shows that in certain projectile/target combinations it is not enough just to pass the one-dimensional potential-energy barrier in order to form a compound system, but an "extra push" is required. Once the reactants pass inside a saddle point in the complex multi-dimensional configuration space, fusion is considered to have occurred. It is generally assumed that the system equilibrates rapidly and the subsequent decay can be described within the framework of the statistical model.

However, neutron multiplicity measurements [2] showed first evidence for entrance channel dependent effects in the decay of compound nuclei. In a recent measurement of high energy γ-rays of the fusion evaporation reactions $^{16}O + ^{148}Sm$ and $^{64}Ni + ^{100}Mo$, it was observed that the γ-ray spectrum from the more symmetric reaction could not be described within the standard statistical model [4]. Figure 1 shows the γ-ray spectra for the two reactions (^{16}O (a), ^{64}Ni (b)) including the fits of the statistical model calculations.

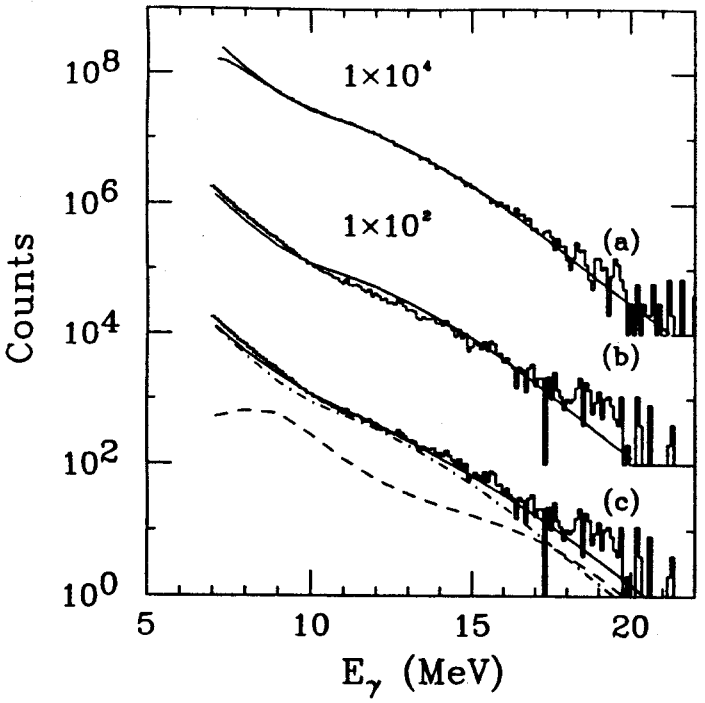

Figure 1: Comparison of the γ-ray spectra from ^{164}Yb following the reaction $^{16}O + ^{148}Sm$ (a) and $^{64}Ni + ^{100}Mo$ (b) and (c). The solid curves are calculations using the code CASCADE. Part (c) shows the calculation which included contributions from the formation (dashed) and the compound nucleus (dot-dashed) decay.

Fig. 2 (a) shows the quality of the fit of the ^{16}O data (■) and the large discrepancy for the ^{64}Ni data (◇) in a linearized plot. To create this plot, the data as well as the calculations were divided by the same spectrum calculated using a constant dipole γ-ray strength function.

The compound nucleus ^{164}Yb was formed in both reactions at an excitation energy of 49 MeV and a

multiplicity filter was used to select the population of similar angular momenta. The possibility of contribution from other than fusion evaporation reactions to the γ-ray spectrum of the more symmetric reaction was carefully considered. However, for example neither fission nor deep inelastic scattering could explain the discrepancy.

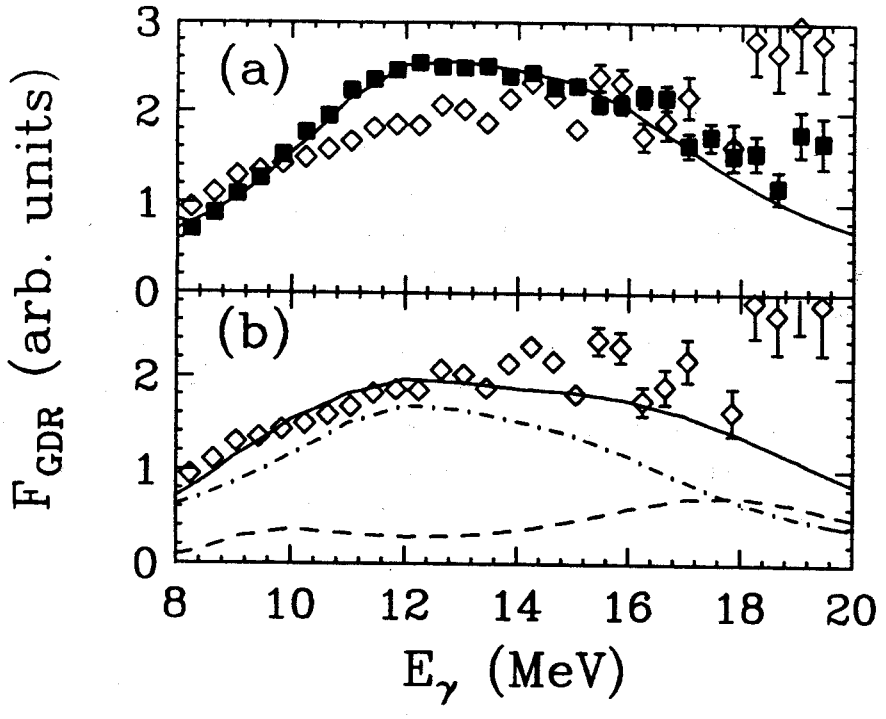

Figure 2: Linearized plots of the γ-ray spectra from the ^{16}O (■) and ^{64}Ni (◇) induced reactions. The data as well as the calculations (solid lines) were divided by the same constant strength function. The calculation shown in (a) is for the ^{16}O data, the calculation for the ^{64}Ni data is essentially identical. The total calculated spectrum in (b) is a sum of contributions from the formation (dashed) and the compound nucleus (dot-dashed) decay.

Thus, we explored the possibility that differences in the formation process of the two reactions could produce the different spectral shapes. According to the semi-classical dissipative collision code HICOL [5], the ^{16}O-induced reaction reaches equilibrium quite rapidly ($\sim 10^{-21}$s) in the shape and thermal energy degrees of freedom tracked by the code. The calculated approach to equilibrium is much slower ($\sim 10^{-20}$) for the ^{64}Ni reaction. This "formation time" for the ^{64}Ni + ^{100}Mo is, in fact, comparable to the mean time for neutron evaporation. If neutrons and γ rays are emitted during this prolonged formation time, a modification of the resulting emission spectra compared to those measured with ^{16}O + ^{148}Sm is not surprising.

To establish a qualitative idea of this effect which might be expected, we have attempted to model this non-equilibrium decay picture using a step-wise application of the equilibrium statistical model in the form of the code CASCADE. According to calculations with HICOL, key parameters (thermal energy, composite system shape, etc.) of the statistical model are changing during the formation time. We treat this by dividing the formation time into time steps, using fixed statistical model parameters obtained from the appropriate time averaged HICOL result for each step, allowing decays to occur within the time step, and obtaining the input population distributions for each step from the results of the preceding steps. The final step is a conventional equilibrium statistical calculation with decay proceeding without a time cutoff. For present purposes, the simplest (i.e. two-step) implementation of this scheme is adequate as an illustration. We take the mean excitation energy (30 MeV) and deformation parameters from the HICOL calculation. The GDR parameters derived from these HICOL results are $E_1 = 9.2$ MeV and $E_2 = 18.0$ MeV. The corresponding widths are estimated as $\Gamma_1 = 3.0$ MeV

and $\Gamma_2 = 6.0$ MeV. A level density parameter of A/15 was chosen, guided by level densities for superdeformed shapes [6]. The first (formation) step lasts for $\sim 2 \times 10^{-20}$s. A rigorous extraction of the uncertainty in this formation time is difficult; we estimate a value of $^{+2}_{-1} \times 10^{-20} s$. The resulting populations in excitation energy and spin were taken as input for the next (fully equilibrated) step, which was treated within the regular statistical model using the standard parameters [3]. Results of these calculations are shown in Fig. 1 (c) and 2 (b) in comparison with the ^{64}Ni data. The total γ-ray spectrum (solid) is a sum of two contributions: γ rays emitted during the formation time (dashed) and γ rays from the compound nuclei (dot-dashed).

The main difference in the spectral shape between the regular statistical model and including the formation time effect is not additional γ rays from the formation phase, as can be seen in Fig. 1 (c). The main effect depends on the fact that the branching ratio for emission of high-energy γ rays (i.e. E_γ near the GDR peak) is a strongly increasing function of increasing excitation energy. The reduced effective excitation energy during the formation time therefore results in a reduced high energy γ-ray yield during the initial step. The cooling of the compound nucleus due to particle evaporation during the formation stage results in a lower mean energy and, hence, a modification of the γ-ray spectrum resulting from the compound system after full equilibration. It is worth noting that those γ rays emitted during the formation stage sample a quite different dipole strength function from that of the compound system.

In conclusion, we could explain the observed large differences in the γ-ray spectra following the decay of the compound nucleus ^{164}Yb when formed with two reactions, by assuming long formation times ($\sim 2 \times 10^{-20}$s) for the ^{64}Ni + ^{100}Mo system compared to the reaction ^{16}O + ^{148}Sm.

a. Oak Ridge National Laboratory, Oak Ridge, Tennessee.
b. Dept. of Chemistry, Washington University, Missouri.
c. KFA, Jülich, Germany.

References

1. W. J. Swiatecki, Physica Scripta **24**, 113 (1981).
2. W. Kühn, P. Chowdhury, R. V. F. Janssens, T. L. Khoo, F. Haas, J. Kasagi, and R. M. Ronningen, Phys. Rev. Lett. **51**, 1858 (1983).
3. M. Thoennessen *et al.*, in "Nuclear Structure and Heavy Ion Dynamics 1990", Edited by R. R. Betts and J. J. Kolata, Institute of Physics Conference Series 109, Adam Hilger, 1991.
4. H. Feldmeier, Rep. Prog. Phys. **50**, 915 (1987).
5. K. Schiffer and B. Herskind, Nucl. Phys. **A520**, 521c (1990).

SEARCH FOR HIGH ENERGY TARGET EXCITATIONS THROUGH INELASTIC ALPHA SCATTERING.

E. Ramakrishnan, A. Azhari, R. A. Kryger, R. Pfaff, M. Thoennessen, S. Yokoyama, J. R. Beene[a], F. E. Bertrand[a], P. E. Mueller[a], G. Van Buren[b], R. J. Charity[b], P-F. Hua[b], D. G. Sarantites[b] and L. G. Sobotka[b].

The high energy region beyond the giant resonances built on the ground state in inelastic heavy-ion scattering is still not understood. The continuum could correspond to high target excitations or it could be predominantly due to other processes such as projectile pickup and sequential decay [1], or nucleon and cluster knock out [2]. Recently, light particle coincidence experiments were performed in order to investigate the origin of the continuum [3].

If the target is actually highly excited by inelastic scattering, it equilibrates rapidly and these excited states should decay statistically. Thus, in a coincidence measurement of high energy γ rays with the scattered projectile, one should be able to observe the γ-ray decay of the giant dipole resonances (GDR) built on these highly excited states [4].

In a recent γ-ray coincidence measurement of 84 MeV/A ^{17}O on a ^{208}Pb target, the high energy γ-ray spectrum showed enhancement around 13 MeV, where the GDR built on excited states of ^{208}Pb is expected to be located [5]. This observation of the GDR is evidence for target excitation through inelastic excitation.

In order to investigate the continuum in more detail, we performed a γ-ray coincidence measurement. A 3 mg/cm^2 thick ^{208}Pb target was bombarded with a 40 MeV/A α beam from the K1200. The inelastically scattered projectiles and other light charged particles were detected using the Washington University *Dwarf Ball/Wall* 4π CsI array [6]. High energy γ rays were measured in coincidence using 76 BaF_2 detectors from the ORNL array and 19 BaF_2 detectors from NSCL. These were arranged in 5 close-packed arrays of 19 detectors each.

Figure 1 shows the singles (a) and coincidence (b) α spectra from a forward ring (23°) of the Dwarf Wall. The elastic peak at $\sim$ 160 MeV contains the low energy excitations, due to energy resolution of $\sim$ 2 % of

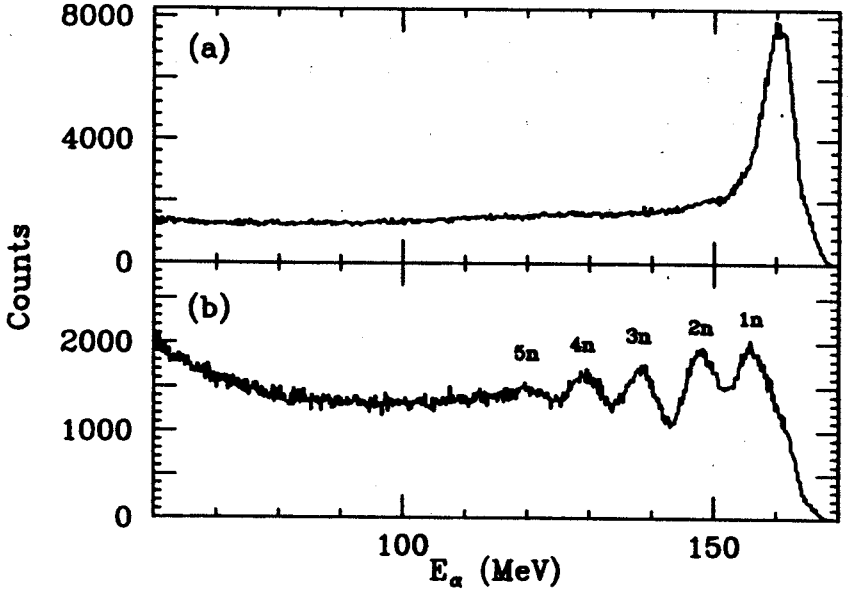

Figure 1: Singles (a) and γ-ray coincidence (b) α spectra from the Dwarf Wall forward ring at 23°.

the CsI detectors. In the singles spectrum there is evidence around 12 MeV for giant resonances built on the ground state. At higher energies, the spectrum is featureless. The α spectrum in coincidence with γ-rays ≥ 4 MeV shows structures up to $\sim$ 50 MeV excitation energy (corresponding to E_α =110 MeV). These peaks result from the opening of successive neutron evaporation channels in the statistical decay of the excited target nucleus, and are evidence for strong target excitation contributions up to at least 50 MeV.

The high energy γ-ray spectra from a preliminary analysis of a subset of the data are shown in figure 2. These spectra are in coincidence with α particles detected at forward angles (14°-31°) in the Dwarf Wall array. The spectra were obtained by gating on inelastic α energies of 60 - 70 MeV and 100 - 110 MeV, which correspond to target excitation energies of 90 - 100 MeV (solid) and 50 - 60 MeV (dotted) respectively. The γ-ray energies were summed for each individual array, and the five spectra of the arrays were then added together. Contributions from neutrons were eliminated via time of flight and random coincidences were subtracted from the data.

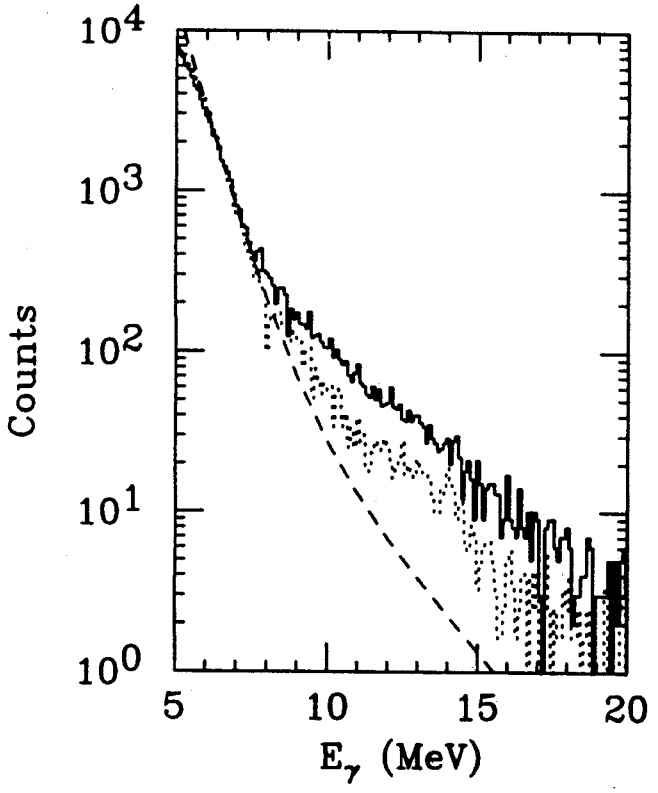

Figure 2: High energy γ-ray spectra in coincidence with inelastically scattered projectiles, gated on target excitation energies of 90 - 100 MeV (solid) and 50 - 60 MeV (dotted). The dashed curve is the result of a statistical model calculation with no GDR strength function. The spectra were normalized in the range of 6 - 7 MeV.

The enhancement in γ-ray strength around 13 MeV is clearly seen for the 50 - 60 MeV excitation energy range (dotted). The dashed curve is the result of a statistical model calculation which does not include the GDR strength function. The enhancement is even more pronounced in the spectrum gated on higher excitation energies (solid). Again this is evidence for strong contributions from high energy target excitations, since the probability of GDR decay increases with excitation energy in an equilibrated excited nucleus.

The preliminary analysis has shown that the inelastic continuum in the particle spectrum has strong contributions from target excitation. Now that we have established those contributions, it is possible to extract

the details of the GDR as a function of excitation energy. Since inelastic scattering does not excite large angular momenta, this method allows us to study the evolution of the GDR as a function of excitation energy, decoupled from angular momentum effects.

The final data analysis and the statistical model calculations are in progress.

a. Oak Ridge National Laboratory, Oak Ridge, Tennessee.
b. Dept. of Chemistry, Washington University.

References

1. H. G. Bohlen *et al.*, Z. Phys. A **320**, 237 (1985).
2. N. Matsushita *et al.*, Nucl. Phys. A **410**, 327 (1983).
3. Y. Blumenfeld, Michigan State University Report No. MSUNSCL-685, 1989 (unpublished), p. 32; N. Frascaria, *ibid.*, p. 53.
4. K. A. Snover, Ann. Rev. Nucl. Part. Sci. **36**, 545 (1986).
5. M. Thoennessen *et al.*, Phys. Rev. C **43**, R12(1991).
6. D. W. Stracener *et al.*, Nucl. Instr. and Meth. A294(1990).

PROTON DECAY FOLLOWING THE HEAVY ION TRANSFER REACTION $^{90}Zr(^{7}Li,^{6}He)^{91}Nb^{*}$

G.H. Yoo, G.M. Crawley, J. Kelley, N.A. Orr, J.S. Winfield, J.E. Finck[a], S. Gales[b] and H. Laurent[b]

In single nucleon stripping reactions, substantial backgrounds have been observed at high excitation energies [1,2]. They made it difficult to extract information about the states of high excitation. These backgrounds must be removed to understand the states at high excitation. One of the ways to exclude these backgrounds is to detect a charged particle emitted in the backward direction from the excited residual nucleus in coincidence with the ejectile.

The proton decay of continuum states in ^{91}Nb excited by the single proton stripping reaction $^{90}Zr(^{7}Li,^{6}He)$ at 50 MeV/nucleon was measured and compared with theoretical predictions. The ^{6}He ejectiles were detected at zero degrees in the focal plane of the A1200 which was used as a 0^{o} spectrograph with an angular acceptance of 3^{o}. The charged particles emitted from the excited residual ^{91}Nb nuclei, mainly protons, were observed at the backward angles. The focal plane detector system consisted of two position sensitive Si detectors (1 mm thick, 1 cm tall and 5 cm long) in series and separated by 1 cm, and the backward angle array consisted of three Si PIN diodes (0.38 mm thick, 3 x 3 cm^2) which were coated with Al(1.4μm) on one side and with Au(0.4μm) on the other side. This array was located 10 cm away from the target, arranged between 150^{o} and 165^{o}, and had a total solid angle of 0.27 sr.

The ^{6}He spectra for the coincidence measurement of $^{90}Zr(^{7}Li,^{6}He,p)$ reaction obtained at zero degrees are displayed in Fig. 1 as well as a ^{6}He singles spectrum. The total spectrum, which consists of true and random events, was obtained by gating on the true plus random peak in the time spectrum; the random spectrum was obtained by gating on one of random peaks; and the true spectrum is obtained by subtracting the random spectrum from the total spectrum. In each case, the excitation energies corresponding to the proton and neutron thresholds (B_p = 5.15 and B_n = 12.06 MeV each) are marked with arrows.

In the singles spectrum, broad peaks are observed at excitation energies 6.5 and 9.5 MeV above the continuum states. They appear to be the single particle states rather than the resonance states, formed by the transfer of a single proton from ^{7}Li to ^{90}Zr. The sharp peak at about 12 MeV is an IAS (Isobaric Analog State). No other peaks are seen at excitation energies above 12 MeV. In the true spectrum, the cross section increases from 9 MeV to 12 MeV, and then decreases rapidly to about 10% of the peak. No structure is observed below 9 MeV even though the proton threshold is 5.15 MeV. Peaks seen near 6.5 and 9.5 MeV in the singles spectrum are not observed clearly in the coincidence spectrum although these may some residual of the 9.5 MeV peak. The strong suppression of proton emission in this region appears to be caused by the strong Coulomb and centrifugal potential barriers, and most of the decay must be through gamma emission. Since the threshold for the neutron emission is 12.06 MeV, this suggests that once neutron emission is permitted it becomes dominant over the proton and gamma decays.

The calculated cross section for the proton decay from the excited ^{91}Nb nucleus following the proton transfer reaction $^{90}Zr(^{7}Li,^{6}He)$ at excitation energies between 5.15 and 20 MeV are compared to the experimental results. The first part of this calculation is to determine a cross section for the formation of the excited ^{91}Nb nucleus formed by proton transfer. This was done using the Brink-Bonaccorso model [3,4]. The second part is to determine the probability of proton decay from the excited ^{91}Nb nucleus. This was calculated with the computer code CASCADE using the Hauser-Feshbach theory [5,6]. Finally, the two theoretical results are combined to give the cross section for proton decay following the proton transfer reaction.

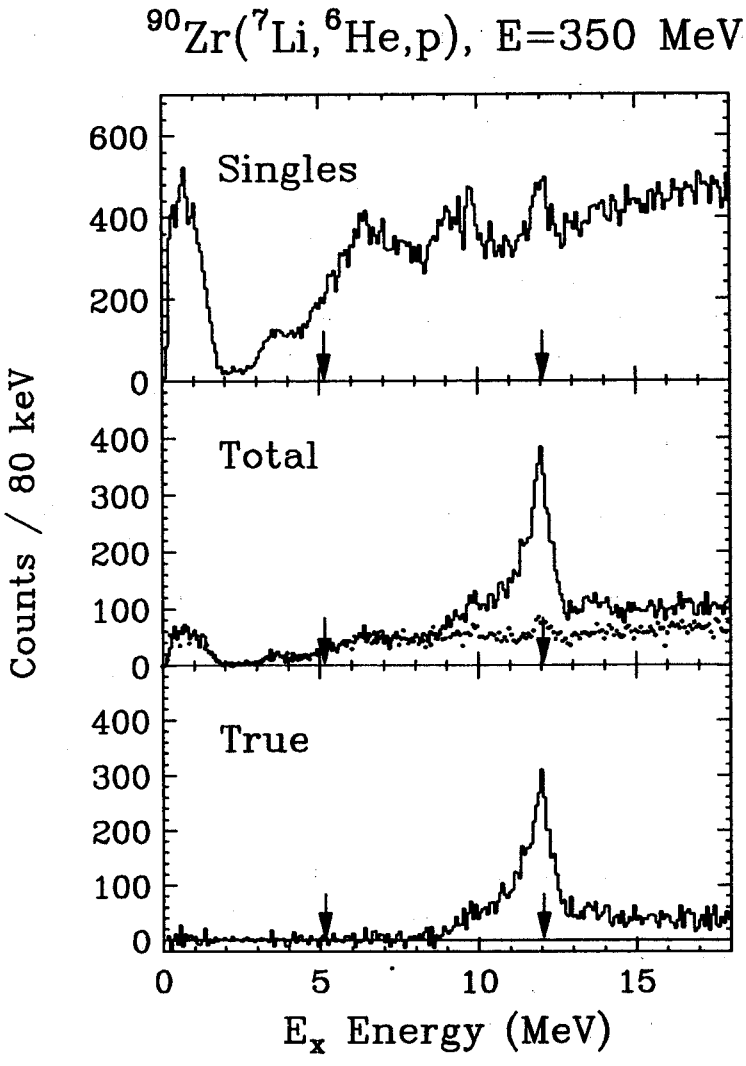

Figure 1: The ^{6}He singles and coincidence spectra for the ^{90}Zr(^{7}Li,^{6}He,p) reaction obtained at zero degrees. Spectrum "Total" includes random as well as true. The solid line represents total, and the dotted line represents random. Spectrum "True" was obtained by subtracting the random spectrum from the total spectrum. The arrows represent the excitation energies in ^{91}Nb corresponding to the proton and neutron thresholds ($B_p = 5.15$ and $B_n = 12.06$ MeV respectively).

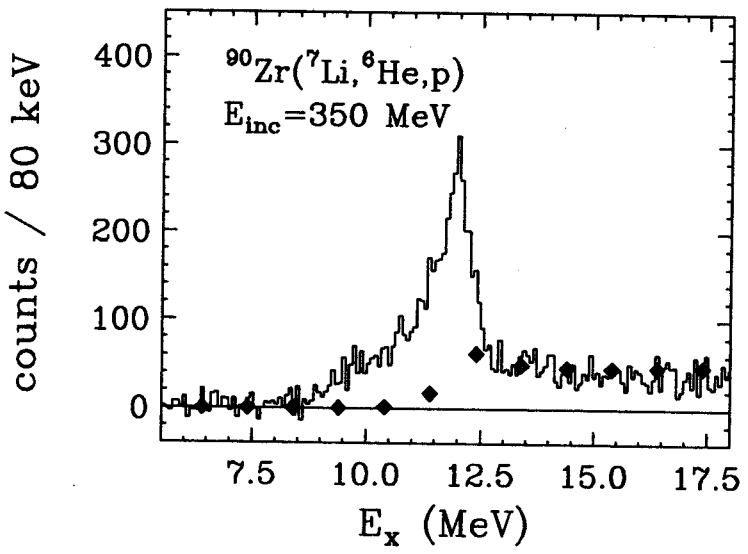

Figure 2: Comparison of the proton decay cross section calculations with the experimental result. The cross sections for the formation of the compound ^{91}Nb nucleus were obtained using the Bonaccorso-Brink theory. The calculated values are normalized to the experimental result at high excitation and are marked by solid diamond.

The cross section $\sigma(E)$ were obtained using the relation

$$\sigma(E) = \sum_{l=0}^{l_{max}} \sigma(E,l)_{p-tr} \cdot \int P(E,l,\epsilon)_{p-decay} d\epsilon, \tag{1}$$

where E and l are the excitation energy and orbital angular momentum of parent's nucleus respectively, and ϵ is the kinetic energy of the emitted proton. $\sigma(E,l)_{p-tr}$ is the cross section for the formation of the compound state determined by the Brink-Bonaccorso model, and $P(E,l,\epsilon)$ is the proton decay probability obtained from the CASCADE calculations. The calculated results using the above equation are given in Fig. 2 as a function of excitation energy of ^{91}Nb. The calculations are normalized to the experimental data at high excitation. The calculations predict that the cross section is almost zero up to 10 MeV of excitation and increases steadily up to 13 MeV and then stays nearly constant.

If the predicted cross sections are normalized to the high excitation energy part of the spectrum, then the predictions significantly underpredict the observed cross section between 9 and 12.5 MeV. In particular since the Brink-Bonaccorso calculations do not predict the strong excitation of the IAS at 12 MeV, they would not be expected to reproduce the strong enhancement of this state seen in the coincidence spectrum. The coincidence spectrum between 9 and 12.5 MeV appears to have two components, a strong sharp symmetric peak near 12 MeV corresponding to the IAS and a broader piece corresponding to continuum states. Preliminary results[7] indicate that a substantial part of the continuum arises from the decay of continuum states as predicted by the Brink-Bonaccorso Model.

a. Central Michigan University, Mt. Pleasant, Michigan
b. Institute de Physique Nucleaire, Orsay, France

References

1. S. Fortier et al., Phys. Rev. C41, 2689(1990)
2. G. Yoo et al., Phys. Rev C 47, 1200(1993)
3. A. Bonaccorso, D. M. Brink and L. Lo Monaco, J. Phys. G 13, 1407(1987)
4. A. Bonaccorso and D. M. Brink, Phys. Rev. C 38, 1776(1988)
5. F. Puhlhofer, Nucl. Phys. A280, 267(1976)
6. W. Dilg et al., Nucl. Phys. A217, 269(1973)
7. G. Yoo, G. M. Crawley and J. S. Winfield, NSCL Annual Report, 76(1991)

DECOUPLING AND DEFORMATION

Wm. C. McHarris, Rahmat Aryaeinejad,[a] Wen-Tsae Chou,[b] Yves X. Dardenne,[c]
Christine V. Hampton, Bin Lian, Wade Olivier, Aracelys Ríos, and R. M. Ronningen

In γ-ray spectra produced by heavy-ion induced reactions in the Ta-Re-Ir region, certain bands stand out as receiving the bulk of the population. An example of this is shown in Fig. 1, a "singles" (but requiring a multiplicity of four or greater) spectrum produced by the ^{165}Ho(^{16}O,6nγ)^{175}Re reaction. The labeled peaks originate from the $\pi h_{9/2}1/2^-$[541] decoupled band in ^{175}Re. The summed-gated spectra shown in Fig. 2 illustrate that this band's population intensity is remarkably independent of entrance-channel effects, remaining constant in reactions induced by ^{16}O, ^{20}Ne, and ^{40}Ar; this pattern has been confirmed by other investigators.[1,2] In Fig. 3 we show the level scheme of ^{175}Re, including this decoupled band (Band I), a highly-compressed band based on the $\pi h_{11/2}9/2^-$[514] state (Band II), a possible forked branch of the decoupled band (Band III), and a less-distorted band based on the $\pi d_{5/2}$ 5/2$^+$[402] state.

Decoupled bands are $\Delta I = 2$ bands, low-Ω bands derived from high-j states. As a result, they have very large decoupling parameters. (For an $\Omega = 1/2$ band, the decoupling parameter is the diagonal coriolis matrix element, $\left\langle \left| (\hbar^2/2\Im) I_\pm j_\mp \right| \right\rangle = (\hbar^2/2\Im)\sqrt{I(I+1)-K(K\pm1)}\sqrt{j(j+1)-\Omega(\Omega\pm1)}$.

Examples of these bands (and doubly-decoupled bands in adjacent odd-odd nuclei, where the $\pi h_{9/2}1/2^-$[541] state is coupled with an $\Omega = 1/2$ neutron, most likely the $p_{3/2}1/2^-$[521] state) are shown in Fig. 4.[3] Only the favored signature states are observed experimentally; the other signature is pushed up too high to receive significant population, and the (often unobserved) base states of the odd-mass and odd-odd bands are generally related 3$^+$ in odd-odd systems near 5/2$^-$ odd-mass systems, and 5$^+$ near 9/2$^-$.

A qualitative explanation for the intense population of decoupled bands is straightforward: The most efficient means of handling the large amounts of angular momentum brought in by heavy ions in fusion-evaporation reactions is for the outer nucleons to decouple and line up with the rotation. Thus, the initial states populated should consist primarily of (multiply-) decoupled bands. The γ-ray depopulation then preferentially feeds down through related coriolis-admixed states, ultimately reaching the yrast decoupled bands (or yrast bands having large coriolis matrix elements). This also explains the insensitivity to entrance-channel effects -- although ^{40}Ar undoubtedly populates states of higher angular momentum than, say, does ^{16}O, it is the γ-ray deexcitation "funnel," rather than the initial manifold of states, that determines the observed bands. (In a sense, this explanation is nothing more than multiple-backbending in reverse.)

In other ways, such as band-crossings and alignments, decoupled bands behave predictably. For example, the alignment plots of the Re decoupled bands are compared with those of the corresponding even-even cores in Fig. 5. The downsloping $\pi h_{9/2}1/2^-$[541] state is deformation driving, and, as expected, delays the onset of band crossing in the odd-mass systems. Interestingly enough, a compromise behavior is found in the odd-odd systems.[4] In ^{174}Re and

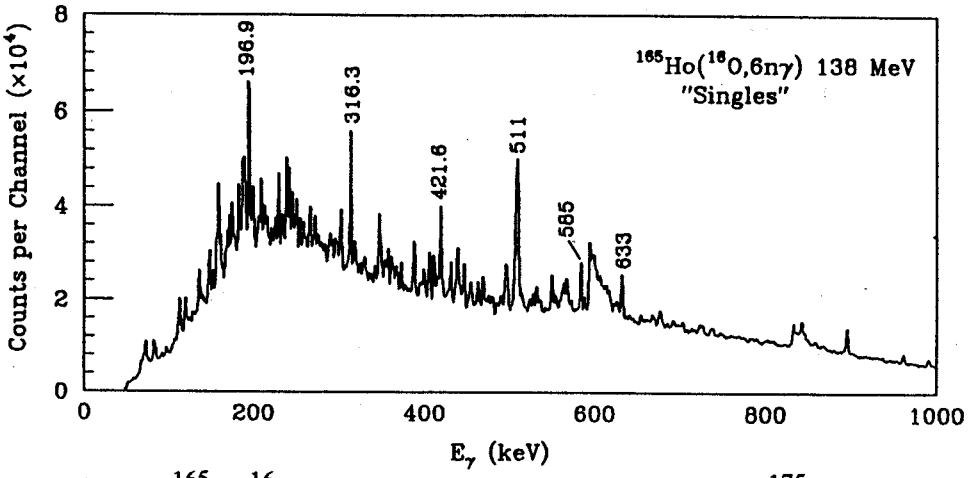

Figure 1. Spectrum from the ^{165}Ho(^{16}O,6$n\gamma$) reaction, showing the decoupled band in ^{175}Re. (Experiment performed at SUNY Stony Brook.)

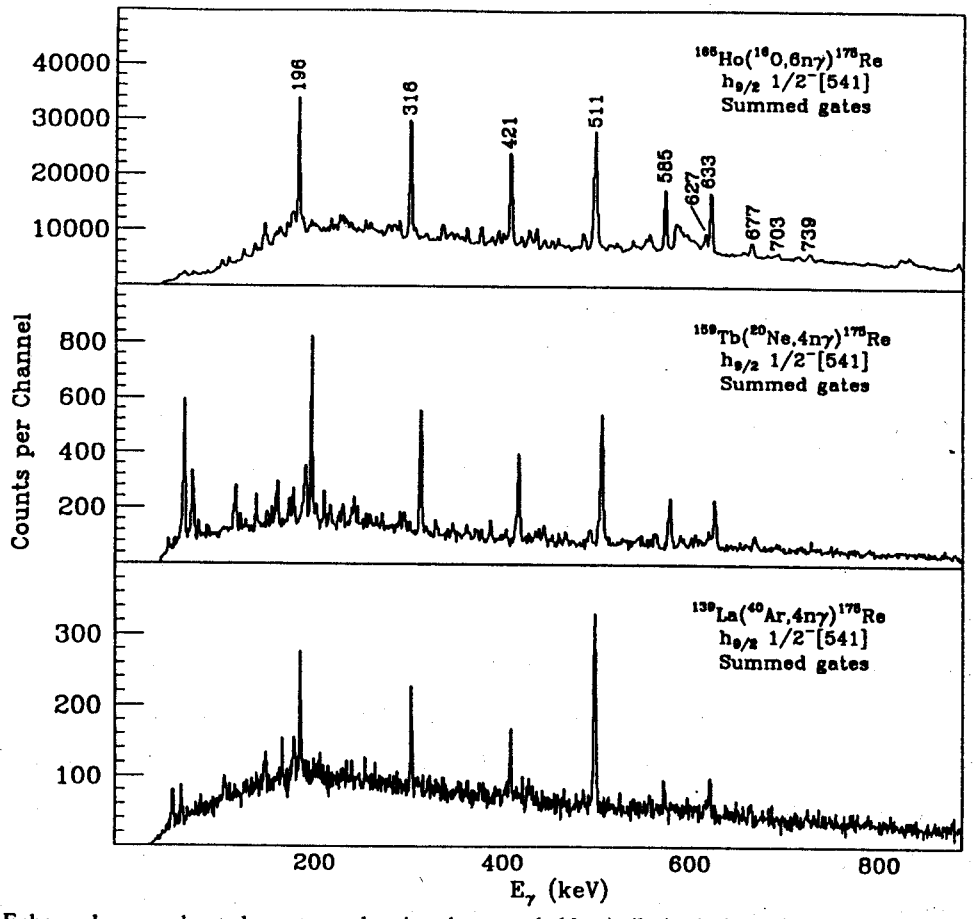

Figure 2. Enhanced summed-gated spectrum showing the remarkable similarity in intensity pattern for the decoupled band in reactions induced by projectiles having significantly different masses.

^{176}Re, the crossing frequencies are essentially the same for the doubly-decoupled bands as for the corresponding cores. Here, the proton states tend toward increasing the crossing frequencies, but the neutron states do the opposite, thus more or less canceling out the effects.

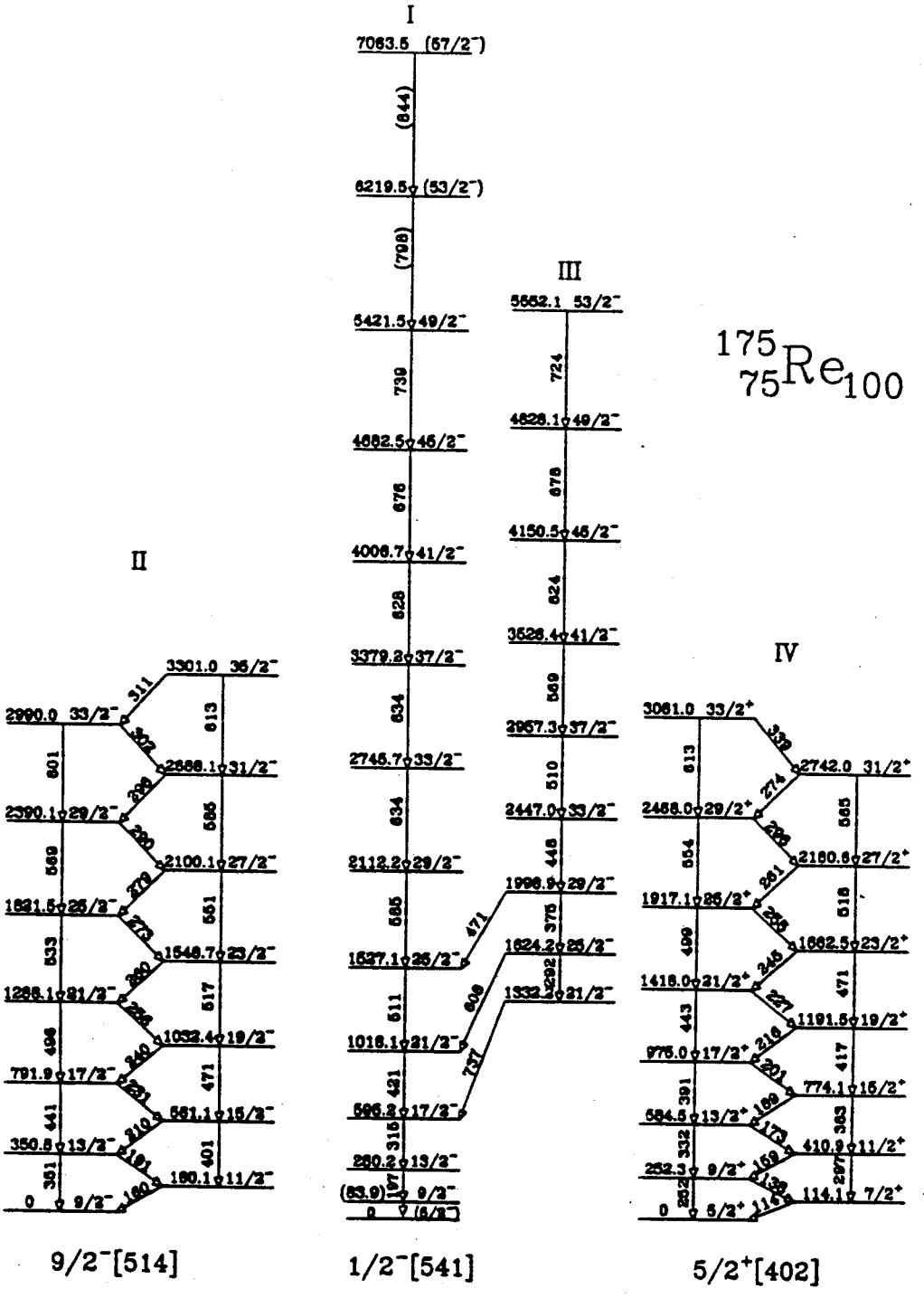

Figure 3. Level scheme of ^{175}Re showing the four most intense rotational bands.

These bands are also well reproduced by interacting boson approximation calculations.[5] Figure 6 shows the results of our calculations for the doubly-decoupled band in ^{176}Re compared with the experimental results. The agreement is striking, especially since the extreme coriolis distortions are reproduced, using no additional free parameters. Again, only the favored signature members of a nominally triplet $K = 1$ band are observed, with the

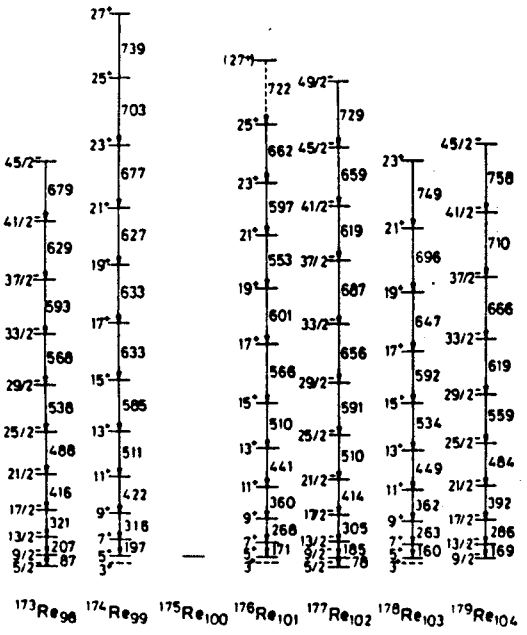

Figure 4. Systematics of decoupled and doubly-decoupled bands in Re nuclei prior to the present work.

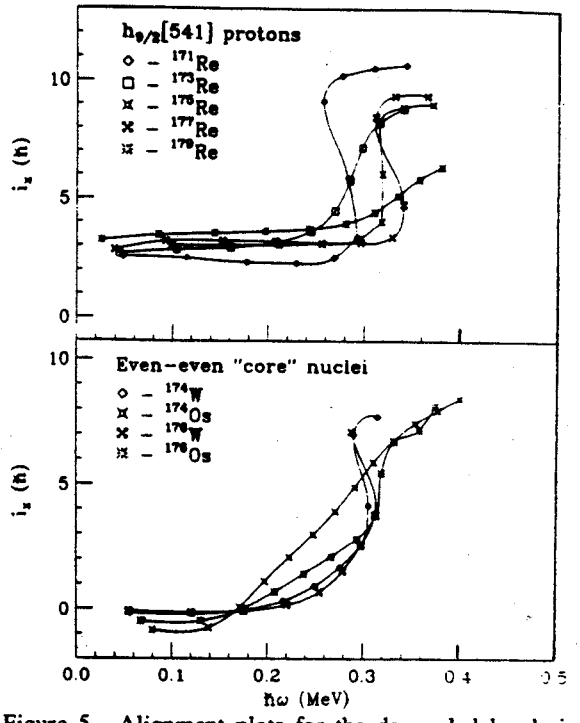

Figure 5. Alignment plots for the decoupled bands in light Re nuclei compared with those of the even-even core nuclei.

unfavored members of this band and those of a singlet $K = 0$ band pushed to higher energies. (Although K is not strictly a good quantum number for decoupled bands, it makes a useful point of reference.)

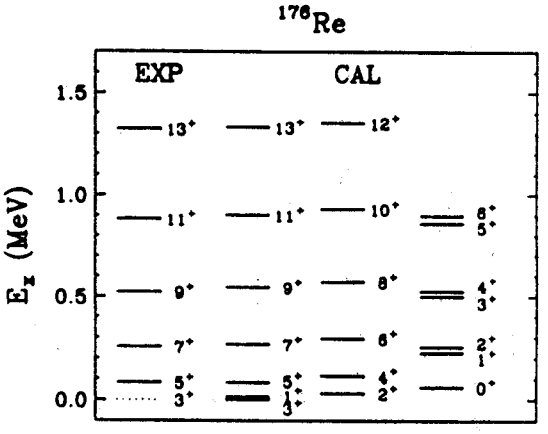

Figure 6. Comparison of the experimentally observed lower-lying members of the doubly decoupled band in ^{176}Re with interacting boson approximation calculations.

We end this short survey with a bit of speculation. Band III in ^{175}Re (Fig. 2) *could* be a fork of Band I, the decoupled band. (It should be emphasized that this is controversial, and other investigators[1,2] have assigned this band as the $pi_{13/2}1/2^+[660]$ state.) There is not room to go into detail, but feeding-intensity arguments and the fact that it feeds across into the decoupled band by enhanced transitions ($E1$'s from a $1/2^+$ band would be highly retarded) well before it reaches its own band-head make it seem related to the decoupled band. And since it has a considerably higher moment of inertia and shows no backbending, it could be a higher-deformation branch of the decoupled band. (Total Routhian surface calculations for nuclei in this region indicate a second prolate minimum.) If so, the simple-minded ideas in Fig. 7 could explain its population behavior.

Finally, in Fig. 8, we show a schematic of the progress of multiple decoupling. Perhaps decoupling is a step on the way toward superdeformation?!

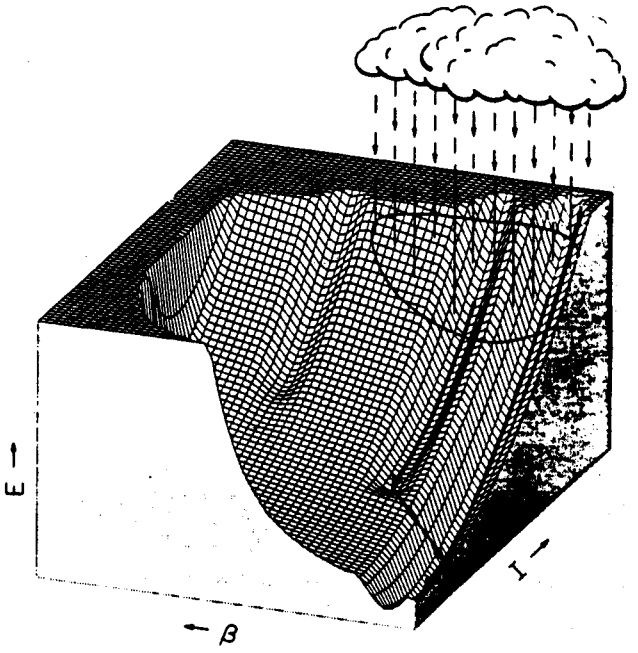

Figure 7. Cartoon-like demonstration of a possible mechanism for a "forked" rotational band. Excitation energy is plotted against both spin and deformation. The cloud represents the manifold of states populated in a fusion-evapoation reaction. These then rain down onto the yrast surface of states, and the higher deformation branch eventually falls into the lower deformation valley.

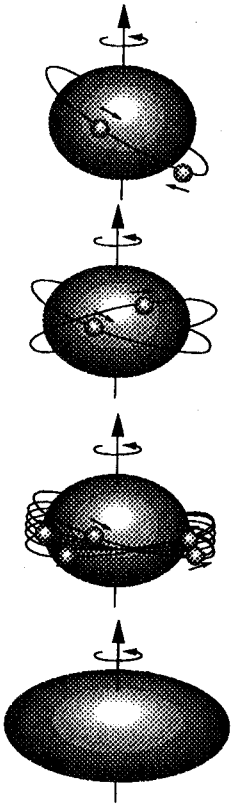

Figure 8. Schematic views of a) a normal strongly-coupled band, b) a doubly-decoupled band, c) a multiply-decoupled band, and d) a superdeformed nucleus. One can speculate that multiple decoupling is a stop on the way to superdeformation.

a. Department of Nuclear Science, National Tsing Hua University, 30043 Hsinchu, Taiwan, ROC
b. EG&G Idaho National Engineering Laboratory, Idaho Falls, ID 83415, USA
c. Nuclear Science Division, Lawrence Berkeley Laboratory, Berkeley, CA 94720, USA

References

1. H.-Q. Jin, L. L. Riedinger, C.-H. Yu, W. Nazarewicz, R. Wyss, J.-Y. Zhang, C. Baktash, J. D. Garrett, N. R. Johnson, I. Y. Lee, and F. K. McGowan, *Phys. Lett.* **B277**, 387 (1992).
2. T. Kibédi, G. D. Dracoulis, F. Fabricius, A. P. Byrne, and A. F. Stuchbery, *Nucl. Phys.* **A539**, 137 (1992).
3. Andrés J. Kreiner, Chapter 26 in *Exotic Nuclear Spectroscopy*, Ed. by Wm. C. McHarris, Plenum Press, 1991.
4. Wade A. Olivier, Wen-Tsae Chou, Aracelys Ríos, Wm. C. McHarris, and Rahmat Aryaeinejad, Chapter 25 in *Exotic Nuclear Spectroscopy*, Ed. by Wm. C. McHarris, Plenum Press, 1991.
5. W.-T. Chou, W. A. Olivier, Wm. C. McHarris, and Olaf Scholten, *Phys. Rev. C* **42**, 221(1990).

γ-RAY SPECTROSCOPY ENHANCEMENT TECHNIQUES

C.V.Hampton, Ben Lian, Jeff Wesley, and Wm.C. McHarris

For years the Fast Fourier Transform (FFT) Technique has been routinely used for noise reduction in many types of spectral analyses, except γ-ray spectroscopy. In nuclear structure experiments using a small number of detectors, the signal-to-noise ratio was increased by compton suppression and/or by extending the data acquisition time. With the advent of the 4π spectrometers, multistep coincidence measurements among a multitude of detectors improves the signal-to-noise ratio but also produces large amounts of white noise within the spectrum. When this is compounded with the necessity to investigate peaks below the 1% intensity level, the need for an additional noise reduction method becomes very apparant.

The data set obtained from the ^{37}Cl on ^{100}Mo reaction, reported in previous annual reports, provides a unique opportunity for development of this technique. For example, most of the peaks of interest in the rotational band structure for the ^{132}Pr nucleus are below the 20% count level and peaks associated with superdeformed bands have considerably lower intensities. A 240 keV gate from a dual gate process for the ^{132}Pr nucleus represents the original data (Figure 1a) at one channel number. Three types of frequency components can be seen: low frequency, observed as a baseline abberation in Figure 1a; high frequency noise; and medium frequency – the γ-ray peaks of interest (Figure 1c). All three are naturally convoluted into a typical spectrum. The objective of an enhancement routine is to remove the low and high frequency components that are not part of the peaks of interest.

To do this, the Oak Ridge User Software was modified to accommodate a discrete FFT program from the IMSL package. This method is preferrable to a smoothing or averaging technique because the peak resolution is not altered with FFT and peaks beneath noise level can actually be seen once the noise frequencies have been removed. The spectra are transformed into the frequency domain, then a limited range of frequencies are chosen to be back transformed into the original domain. An example of the extent of spectral enhancement can be seen in Figure 2: (A) is the original data; (C) is the same data after FFT; and (B) represents the difference between A and C, i.e., the noise that was removed. In order to generate the low- frequency component (baseline spectrum, Figure 1B), another routine was added to the Oak Ridge software – a modification of the Statistics-Sensitive Nonlinear Iterative Peak clipping (SNIP) algorithm that was developed for proton induced X-ray emission spectroscopy.[1] This was preferrable to the baseline spectrum generated by FFT because FFT induced unwanted oscillations in this frequency region. In addition, the Oak Ridge software was modified to adjust the spectral peak intensities automatically for photon transmission through absorbers and multiple detector efficiencies. A cubic spline fitting routine was used to generate percent efficiency at each channel number.

References

1. C.G.Ryan, E.Clayton, W.L.Griffin, S.H.Sie, D.R.Cousens, Nuclear Instru. Methods Phys. Research, B34(1988) 396.

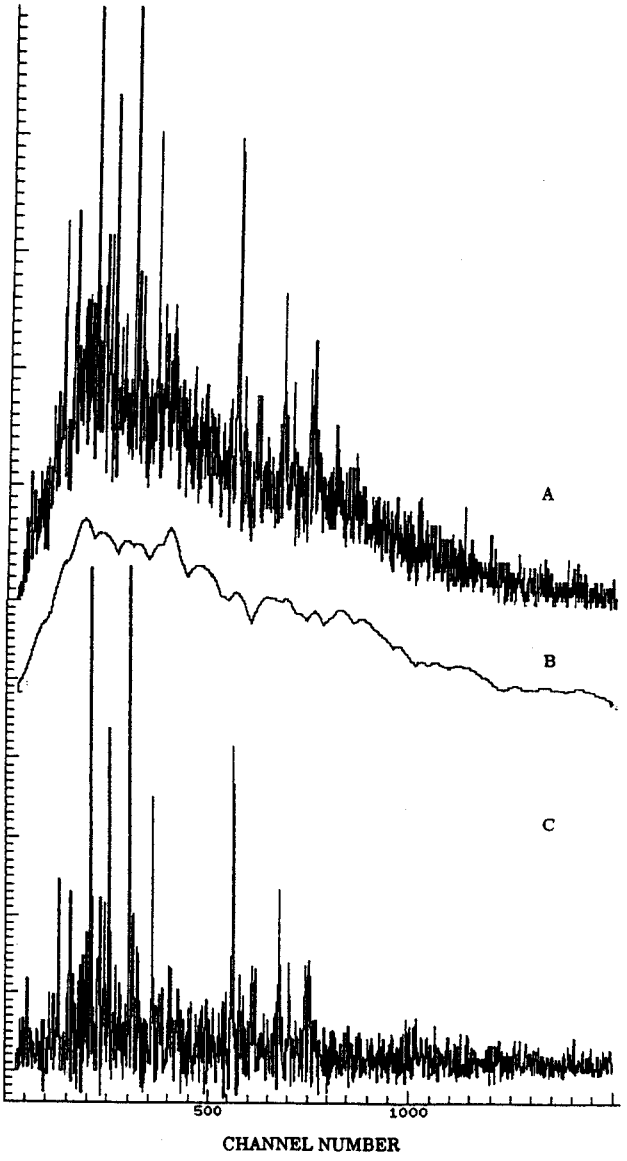

Figure 1:
A: An attenuated spectrum of the original 240 keV gate.
B: Baseline or low frequency noise generated by SNIP.
C: Spectrum after low and some high frequencies were removed.

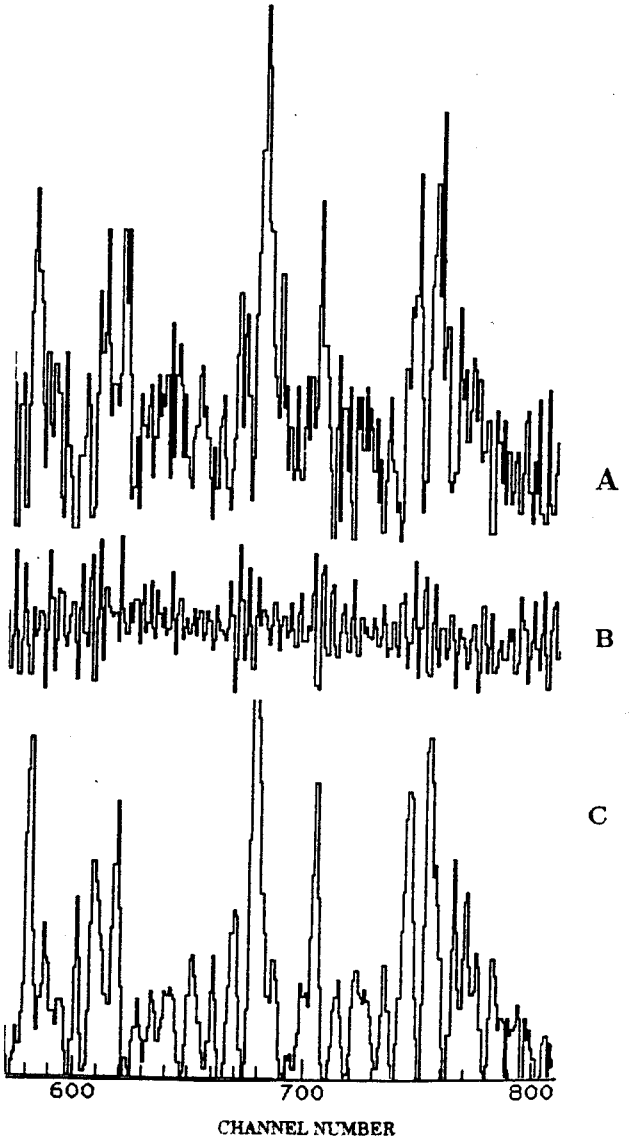

Figure 2:
An expanded view of the 240 keV gate.
A: Original data.
B: Subtracted noise.
C: Data after Fast Fourier Transform.